Electronic Supplementary Information

Unprecedented one-dimensional chain and two-dimensional network dysprosium(III) single-molecule toroics with white-light emission

Li Zhong,‡[a] Wen-Bin Chen,‡[a] Zhi-Jian OuYang,[a] Meng Yang,[a] Yi-Quan Zhang,*[b] Song Gao,*[c] Michael Schulze,[d] Wolfgang Wernsdorfer [d] and Wen Dong*[a]

[a]Guangzhou Key Laboratory for Environmentally Functional Materials and Technology, School of Chemistry and Chemical Engineering, Guangzhou University, Guangzhou 510006, P. R. China

[b]Jiangsu Key Laboratory for NSLSCS, School of Physical Science and Technology, Nanjing Normal University, Nanjing 210023, P. R. China

[c]School of Chemistry and Chemical Engineering, South China University of Technology, Guangzhou 510641, P. R. China

[d]Institute of Nanotechnology (INT), Karlsruhe Institute of Technology, Hermann-von-Helmholz-Platz 1, 76344 Eggenstein-Leopoldshafen, Germany

‡ These authors contributed equally to this work.

Corresponding Authors

E-mail: dw320@aliyun.com (Wen Dong)

E-mail: zhangyiquan@njnu.edu.cn (Yi-Quan Zhang).

E-mail: gaosong@pku.edu.cn (Song Gao)

Experimental section

Materials and General Procedures. All reagents were obtained from commercial sources, and used as received without further purification. Elemental analyses were carried out using a Perkin-Elmer analyzer model 240. IR spectra were recorded as pressed KBr pellets on a Bruker Tensor 27 spectrophotometer with an average of 64 scans. Thermogravimetric (TG) analyses were carried out using Perkin-Elmer TGA4000 thermogravimetric analyzer. Powder X-ray diffraction (PXRD) patterns were carried out on a MiniFlex-600 diffractometer (Cu-Ka, λ= 1.54056 Å) and the calculated patterns were generated with Mercury 3.10. Fluorescent spectra were recorded with an F-7000 fluorescence spectrophotometer. Emission spectra were carried out by employing a neutral filter. The magnetic measurements were performed on the polycrystalline samples using a Quantum Design MPMS3 SQUID-VSM magnetometer. AC magnetic susceptibility data measurements were performed with a 2.5 Oe switching field at frequencies between 1 and 1000 Hz. Diamagnetic correction was performed based on Pascal's coefficients. The single-crystal measurements down to ultralow temperature were performed on a micro-SQUID.

X-ray Crystallography and Data Collection. The crystals were filtered from the solution and suitable crystal is performed in a Rigaku XtaLAB Synergy single crystal diffractometer with graphite monochromated Cu Kα radiation, which is equipped with Oxford Cryosystems low-temperature device, operating at T = 100.00 (10) K. Absorption corrections were applied by using the multi-scan program REQAB. The structures were solved using intrinsic phasing methods (SHELXT). Using OLEX2, data were refined by full-matrix least-squares using SHELXL (2014/7) program packages.[1,2] Anisotropic thermal parameters were applied to all non-hydrogen atoms. Hydrogen atoms were located from difference maps and refined with isotropic temperature factors. There are some lattice water molecules in the structure. However, these water molecules have a large thermal vibration factor. So the crystal data were refined using the SQUEEZE procedure from the PLATON software.[3] Crystallographic Data Centre under reference numbers CCDC 1954138-1354139 for **1** and **2** contain the supplementary crystallographic data for this paper, respectively. The crystal data and collection parameters for **1** and **2** are listed in Table S1.

Synthesis of Complexes 1 and 2.

$[Dy_3(HMBA)(MBA)_3(H_2O)_3(OH)_2]\cdot 10H_2O$ (**1**). H_2MBA (68 mg, 0.4 mmol) and triethylamine (116 mg, 1.16 mmol) dissolved in DMF (2.25 mL). Then $Dy(NO_3)_3\cdot 6H_2O$ (137 mg, 0.3 mmol) was dissolved in distilled water (2.25 mL). The above solution was mixed and then stirred for 2 hours. Block colorless crystals were obtained by slow evaporation of the solution in 29% yield. Elemental analysis calcd (%) for **1** of ($C_{32}H_{53}Dy_3O_{31}$): C, 27.04; H,

3.76. Found: C, 27.07; H, 3.85. FT-IR (KBr, cm^{-1}): 3357 (m), 1656 (s), 1585 (s), 1544 (s), 1394 (s), 1255 (s), 1043 (m), 856 (w), 758 (m).

$[Dy_6(MBA)_6(OH)_4(H_2O)_8](OH)_2 \cdot 33H_2O$ (**2**). H_2MBA (68 mg, 0.4 mmol) and triethylamine (131 mg, 1.31 mmol) dissolved in DMF (2 mL). Then $Dy(NO_3)_3 \cdot 6H_2O$ (365 mg, 0.8 mmol) was dissolved in distilled water (4 mL). The above solution was mixed and then stirred for 2 hours. After slow evaporation of the solution, block colorless crystals were obtained in 24% yield. Elemental analysis calcd (%) for **2** of ($C_{48}H_{124}Dy_6O_{71}$): C, 20.50; H, 4.44. Found: C, 20.48; H, 4.51. FT-IR (KBr, cm^{-1}): 3380 (m), 1608 (m), 1546 (s), 1384 (s), 1255(s), 1207 (m), 1047 (w), 752 (w).

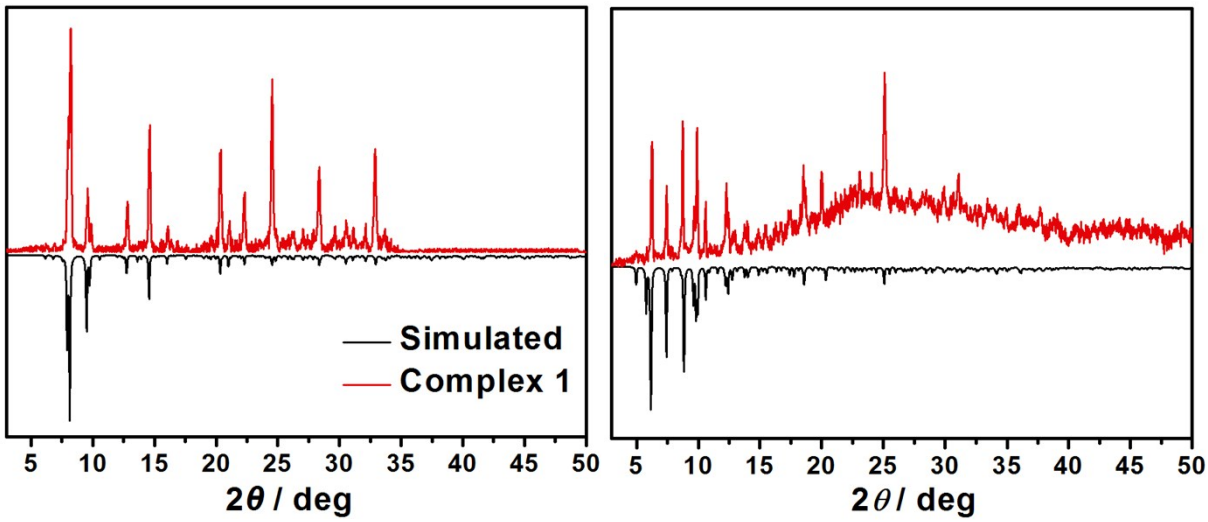

Fig.S1. Powder X-ray diffraction (PXRD) patterns for complexes **1** (left) and **2** (right).

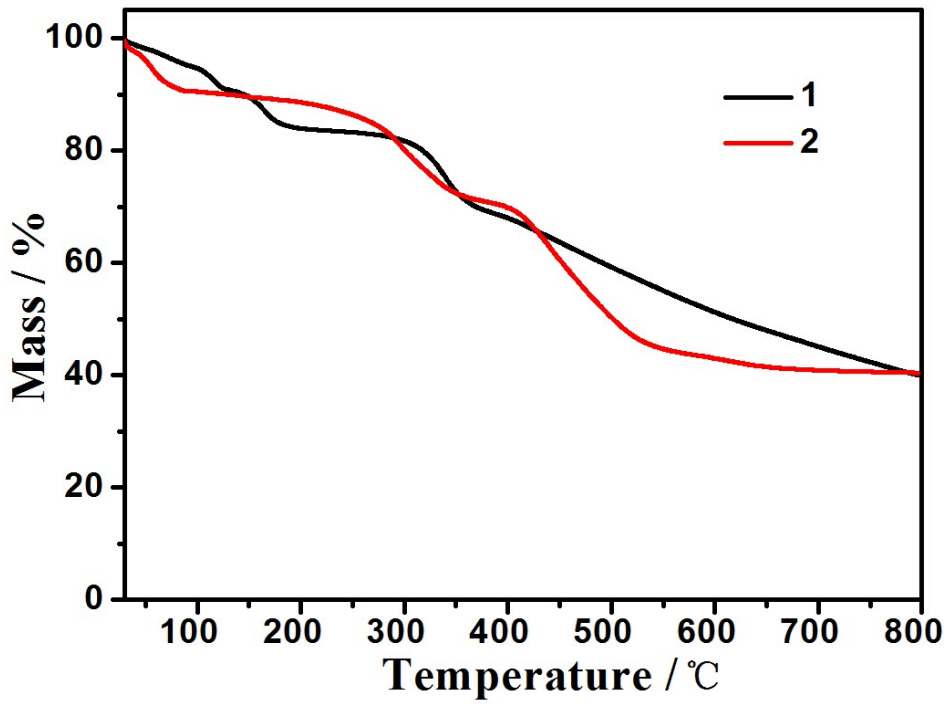

Fig.S2. Thermal gravimetric Analyses (TGA) curves for complexes **1** and **2**.

Table S1. Crystal data and structure refinement for complexes **1**-**2** at 100 K

Complex	**1**	**2**
Empirical formula	$C_{32}H_{53}Dy_3O_{32}$	$C_{48}H_{122}Dy_6O_{69}$
Formula weight	1437.24	2778.40
Crystal system	monoclinic	triclinic
Space group	C2/c	$P\bar{1}$
a / Å	24.2940(2)	15.0529(5)
b / Å	18.1452(2)	16.5502(5)
c / Å	22.5707(2)	19.5506(5)
α / °	90	66.985(3)
β / °	105.5380(10)	74.839(3)
γ / °	90	78.055(3)
V / Å^3	9585.97(16)	4296.7(3)
Z	8	2
ρcalcd (g/cm^3)	1.777	1.767
μ (mm^{-1})	25.276	28.869
F(000)	4896.0	2150.0
Reflections collected	35482	56977
Independent reflections	9712	17289
R(int)	0.0605	0.1211
Goodness-of-fit on F_2	1.122	1.188
Final R indices [I>2sigma(I)] [a,b]	R_1 =0.0528, wR_2 = 0.1514	R_1 =0.1188, wR_2 = 0.3079
R indices (all data)	R_1 = 0.0583, wR_2 = 0.1551	R_1 =0.1538, wR_2 = 0.3416
Largest diff. peak and hole (e.Å-3)	2.75/-2.07	4.91/-1.83
CCDC	1954138	1954139

[a]$R_1 = \sum||F_o|-|F_c||/\sum|F_o|$. [b]$wR_2 = [\sum w(F_o^2 - F_c^2)^2/\sum w(F_o^2)^2]^{1/2}$

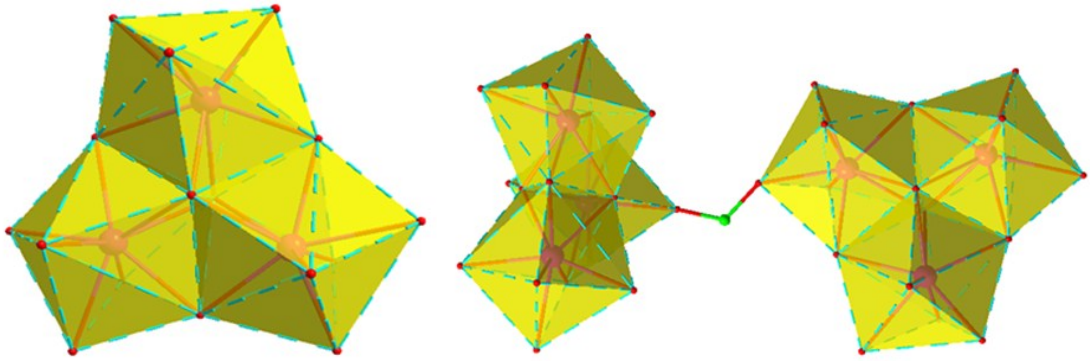

1 **2**

Fig. S3. Coordination geometry of Dy(III) ion in **1**(a) and **2**(b).

Table S2. Complex **1** shape measure (CShM) with SHAPE 2.1 software

	TDD-8 (D2d)	SAPR-8 (D4d)	JBTPR-8 (C2v)	BTPR-8 (C2v)	JSD-8 (D2d)
Dy1	0.61477	2.74282	3.02043	2.49197	2.74153
Dy2	1.17070	1.27608	2.37877	1.80096	3.50041
Dy3	0.69208	2.60315	3.04971	2.69244	3.10889

TDD-8= Triangular dodecahedron; SAPR-8= Square antiprism; JBTPR-8= Biaugmented trigonal prism J50; BTPR-8 = Biaugmented trigonal prism; JSD-8= Snub diphenoid J84.

Table S3. Complex **2** shape measure (CShM) with SHAPE 2.1 software

	TDD-8 (D2d)	SAPR-8 (D4d)	JBTPR-8 (C2v)	BTPR-8 (C2v)	JSD-8 (D2d)
Dy1	0.96257	1.69759	2.51166	2.07359	3.13524
Dy2	0.72690	2.35530	2.98921	2.36552	2.94846
Dy3	0.76610	2.86470	3.10371	2.42495	3.11040
Dy4	0.61586	2.68894	2.69795	2.25971	2.91244
Dy5	0.69910	2.42165	2.88466	2.51045	2.93188
Dy6	0.78343	2.17563	2.63194	2.23216	3.02906

TDD-8= Triangular dodecahedron; SAPR-8= Square antiprism; JBTPR-8= Biaugmented trigonal prism J50; BTPR-8 = Biaugmented trigonal prism; JSD-8= Snub diphenoid J84.

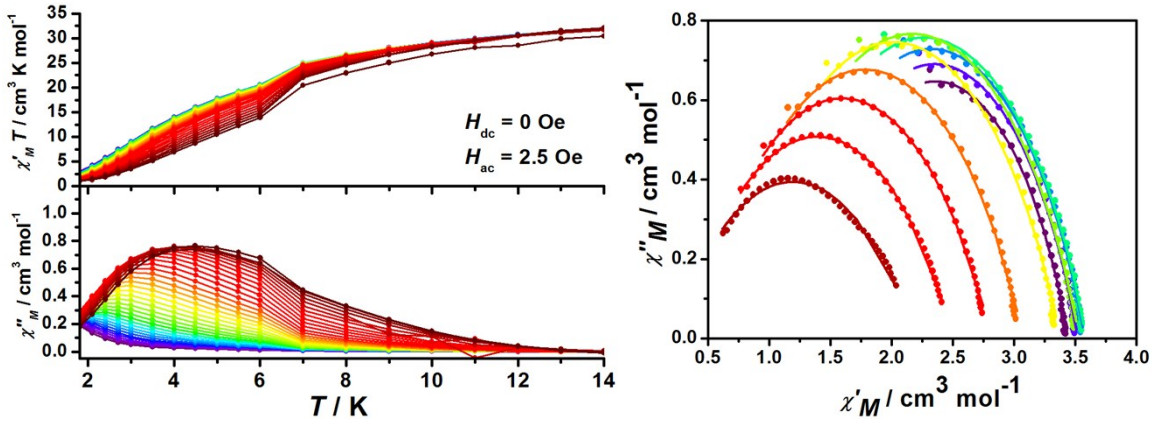

Fig. S4. (left) Temperature dependence of the in-phase $\chi_M'T$ product and out-of-phase χ_M'' for **1** in zero dc field with an AC frequency of 1−1000 Hz. (right) Cole−Cole plots for the ac susceptibilities for **1**. The solid lines are the best fit to Debye's law.

Table S4 Relaxation fitting parameters from Least-Squares Fitting of χ(ω) data for **1** in zero dc field.

T / K	τ	τ	α	α	χ_0	χ_0	χ_∞	χ_∞
	Value	Standard Error	Value	Standard Error	Value	Standard Error	Value	Standard Error
8	1.33E-04	1.29E-05	0.1581	0.02057	3.33064	0.00305	2.45593	0.0499
7	1.40E-04	1.02E-05	0.19454	0.01472	3.56705	0.00322	2.33848	0.04943
6	1.87E-04	7.39E-06	0.31346	0.00685	3.4394	0.00342	1.27618	0.03735
5.5	2.17E-04	8.06E-06	0.32108	0.00676	3.52066	0.00395	1.18035	0.03735
5	2.52E-04	8.65E-06	0.33082	0.0065	3.57751	0.0044	1.06468	0.0362
4.5	2.97E-04	9.34E-06	0.34007	0.00621	3.59053	0.00483	0.93463	0.03426
4	3.64E-04	1.03E-05	0.34879	0.00595	3.53612	0.00523	0.80401	0.03121
3.5	4.64E-04	1.12E-05	0.36345	0.00533	3.37937	0.00524	0.64841	0.02577
3	6.44E-04	1.18E-05	0.38736	0.00422	3.07701	0.00458	0.485	0.01765
2.7	8.24E-04	1.03E-05	0.41332	0.00289	2.81372	0.00333	0.37941	0.01077
2.4	0.00114	8.21E-06	0.45374	0.00164	2.50458	0.00206	0.28317	0.00533
2.1	0.00177	3.87E-05	0.52054	0.00471	2.19188	0.00696	0.19741	0.01336
1.8	0.00373	2.05E-04	0.62715	0.01058	2.02388	0.02427	0.13637	0.02875

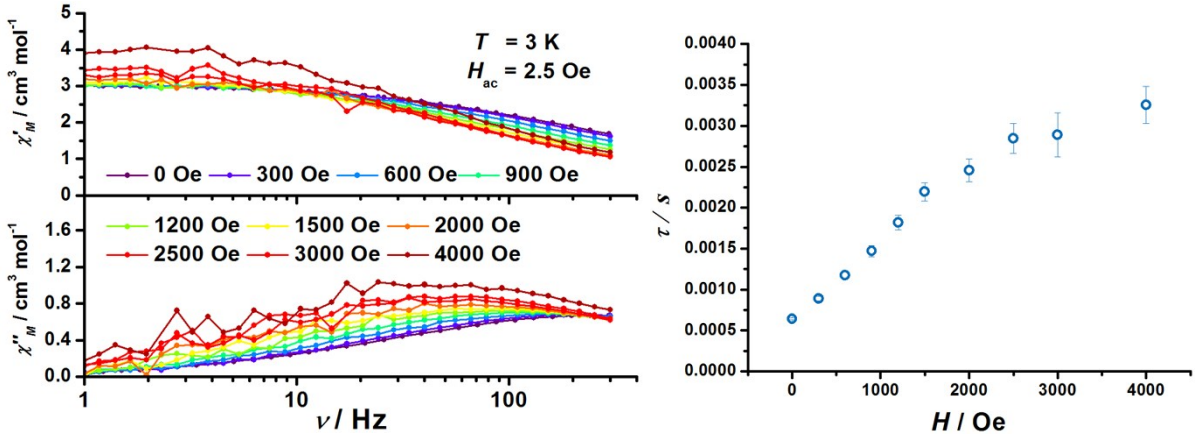

Fig. S5 (left) Frequency dependence of χ'_M and χ''_M signals at various fields at 3 K for **1**. The solid lines are guides to the eyes. (Right) Field-dependent relaxation times for **1** at 6 K.

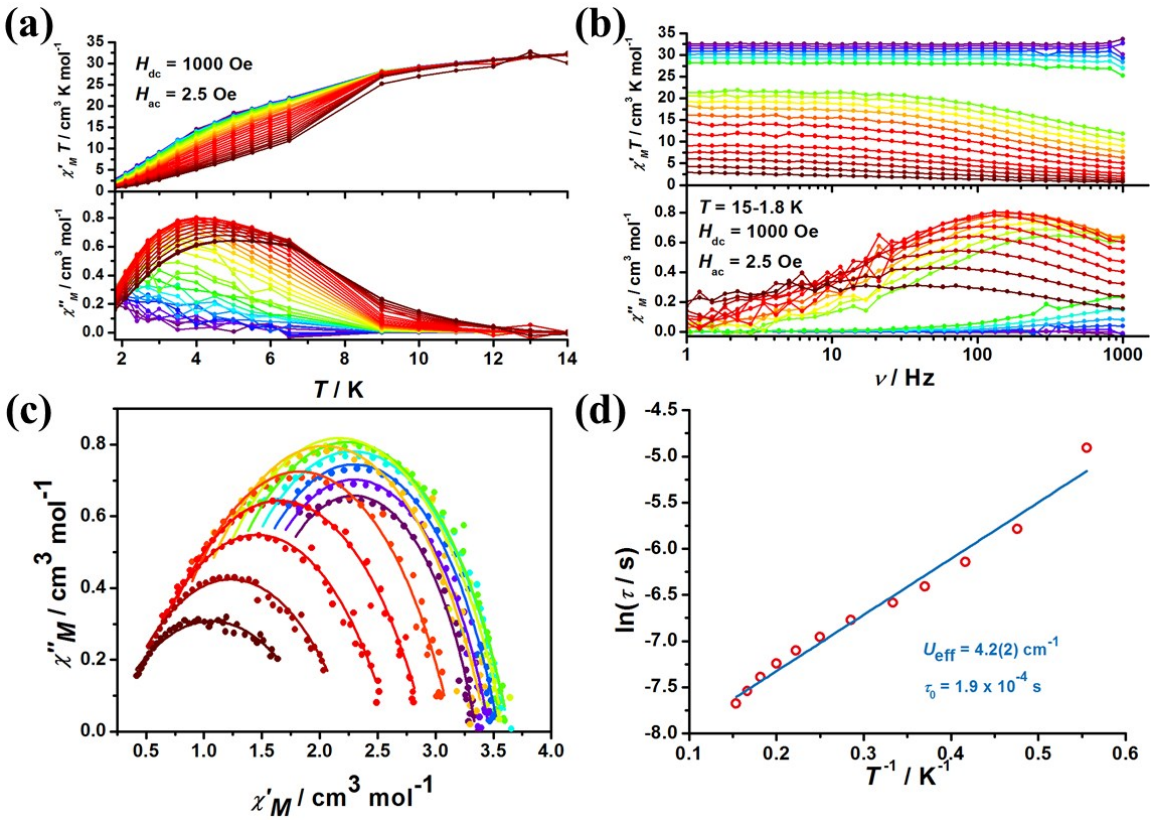

Fig. S6. Alternating current molar magnetic susceptibilities, Cole−Cole plot, and magnetic relaxation for **1**. (a, b) Temperature and frequency dependence of the in-phase ($\chi_M{}'$ T) product and out-of-phase ($\chi_M{}''$) in 1000 Oe dc field for **1** with the ac frequency of 1−1000 Hz. (c) Cole−Cole plot. The solid lines are the best fit to Debye's law. (d) Temperature dependence of the magnetic relaxation time τ under 1000 Oe. The solid lines correspond to a fit to the Arrhenius expression of $\tau^{-1} = \tau_0^{-1} \exp(-U_{eff}/T)$ affording $U_{eff} = 4.2(2)$ cm^{-1} and $\tau_0 = 1.9 \times 10^{-4}$ s.

Table S5 Relaxation fitting parameters from Least-Squares Fitting of χ(ω) data for **1** in 1000 Oe dc field.

T / K	τ	τ	α	α	χ_0	χ_0	χ_∞	χ_∞

	Value	Standard Error	Value	Standard Error	Value	Standard Error	Value	Standard Error
6.5	4.63E-04	2.14E-05	0.289800201	0.012736299	3.348452804	0.009017437	1.24000586	0.043347325
6	5.32E-04	2.05E-05	0.310450218	0.010481683	3.465320233	0.008814683	1.128971095	0.03829833
5.5	6.16E-04	2.30E-05	0.314717821	0.010593154	3.544214568	0.010090644	1.049116897	0.039194084
5	7.14E-04	2.13E-05	0.332336743	0.008411777	3.633761884	0.009291663	0.932482169	0.032609998
4.5	8.23E-04	3.06E-05	0.334613055	0.010902936	3.638593682	0.01315517	0.837953251	0.041702285
4	9.52E-04	3.99E-05	0.337645565	0.012719675	3.596090206	0.016503696	0.740502048	0.047248314
3.5	0.001146087	4.68E-05	0.341778393	0.012884126	3.442328374	0.017520769	0.640938846	0.044251082
3	0.001381122	4.41E-05	0.360483919	0.010037707	3.144234988	0.013946538	0.504918382	0.031305705
2.7	0.001649066	4.24E-05	0.398991149	0.007634036	2.912151098	0.011266549	0.389695794	0.022729412
2.4	0.00214449	6.12E-05	0.43568751	0.008182456	2.614622089	0.012715738	0.302825336	0.021742909
2.1	0.003064199	1.56E-04	0.508877684	0.013060265	2.275435689	0.023490083	0.184189867	0.031969583
1.8	0.007395246	4.84E-04	0.602044817	0.013330985	2.017080136	0.035228962	0.109017313	0.028156015

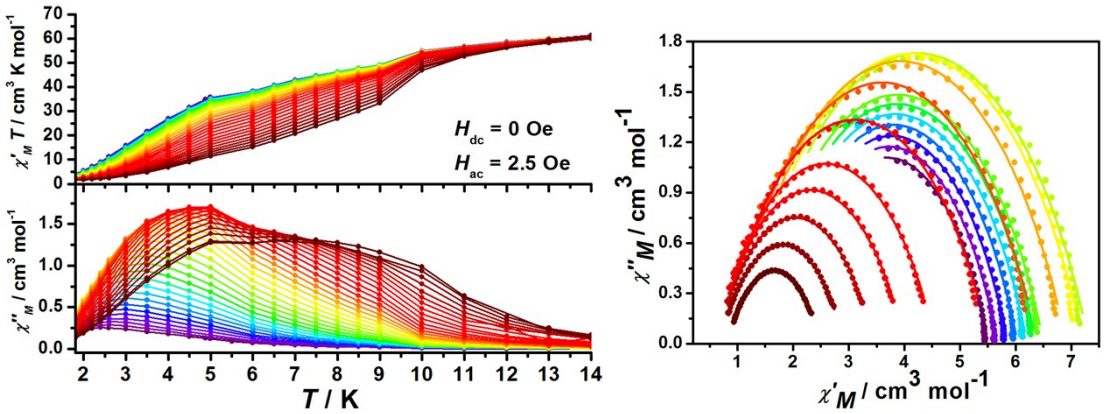

Fig. S7. (left) Temperature dependence of the in-phase $\chi_M'T$ product and out-of-phase χ_M'' for **2** in a zero dc field with an ac frequency of 1−1000 Hz. (right) Cole−Cole plots for the ac susceptibilities for **2**. The solid lines are the best fit to Debye's law.

Table S6 Relaxation fitting parameters from Least-Squares Fitting of χ(ω) data for **2** in zero dc field.

T / K	τ	τ	α	α	χ_0	χ_0	χ_∞	χ_∞
	Value	Standard Error	Value	Standard Error	Value	Standard Error	Value	Standard Error
9	1.68E-04	8.13E-06	0.2961	0.00836	5.48936	0.00645	1.89367	0.0789
8.5	2.07E-04	8.79E-06	0.30965	0.0078	5.67019	0.00734	1.77353	0.07251
8	2.61E-04	1.02E-05	0.31625	0.00783	5.84967	0.00879	1.68816	0.07002
7.5	3.25E-04	1.14E-05	0.32418	0.00756	6.03235	0.01006	1.58679	0.06588
7	4.05E-04	1.28E-05	0.33222	0.00729	6.20705	0.01138	1.47661	0.06211
6.5	5.02E-04	1.40E-05	0.3401	0.00682	6.37062	0.01236	1.36059	0.05686

6	6.25E-04	1.58E-05	0.34404	0.00658	6.50248	0.0136	1.26088	0.05289
5	9.78E-04	1.99E-05	0.34813	0.00605	7.3203	0.01725	1.16068	0.0487
4.5	0.00124	2.24E-05	0.34949	0.00571	7.21341	0.01768	1.04595	0.04244
4	0.0016	2.54E-05	0.34473	0.00509	6.90694	0.01476	0.95342	0.03463
3.5	0.00211	2.88E-05	0.35233	0.00478	6.38746	0.01589	0.80623	0.02711
3	0.00287	3.11E-05	0.35656	0.00392	5.51924	0.01245	0.69356	0.01755
2.6	0.00378	2.93E-05	0.36316	0.00283	4.55358	0.00802	0.62951	0.00955
2.4	0.0044	2.86E-05	0.36787	0.00236	4.00218	0.00608	0.61898	0.0066
2.2	0.00514	2.74E-05	0.37381	0.00192	3.43972	0.00432	0.63553	0.00427
2	0.00601	3.43E-05	0.37981	0.00202	2.91589	0.00382	0.6992	0.00342
1.8	0.00702	5.20E-05	0.38924	0.00255	2.48651	0.00383	0.83076	0.00312

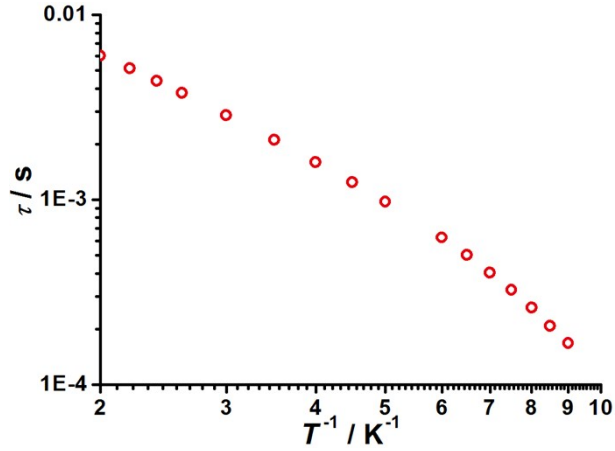

Fig. S8. ln(τ) vs. ln(T) for **2** in a zero dc field.

As shown in the Fig.S8, the ln(τ) vs. ln(T) is not linear dependency, which demonstrate relaxation dynamics is not solely dominated by a Raman process.

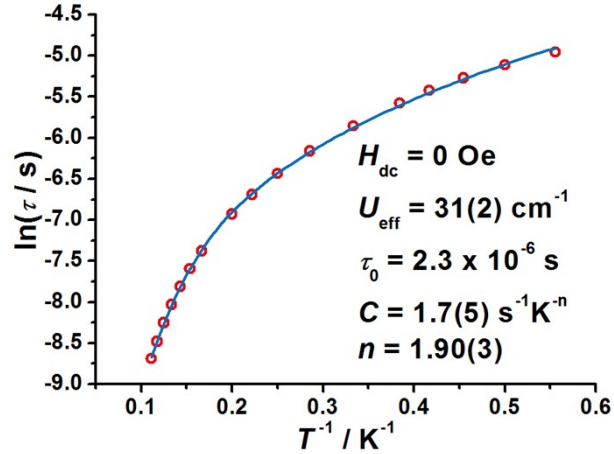

Fig. S9. Temperature dependence of the relaxation time τ in a zero dc field. The solid lines are the best fits to the relaxation equation of $\tau^{-1} = \tau_0^{-1} \exp(-U_{eff}/T) + CT^n$.

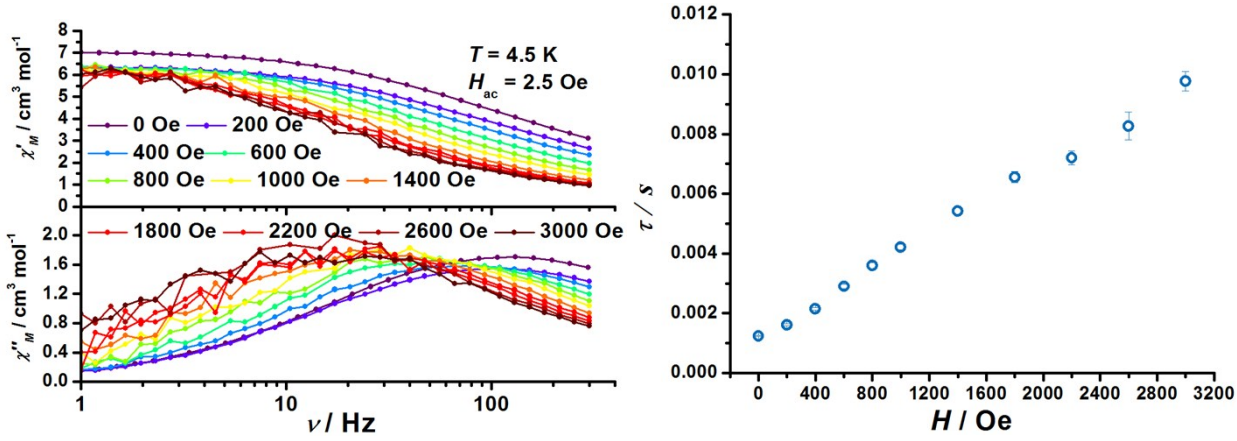

Fig. S10 (left) Frequency dependence of χ'_M and χ''_M signals at various fields at 4.5 K for **2**. The solid lines are guides to the eyes. (Right) Field-dependent relaxation times for **2** at 4.5 K.

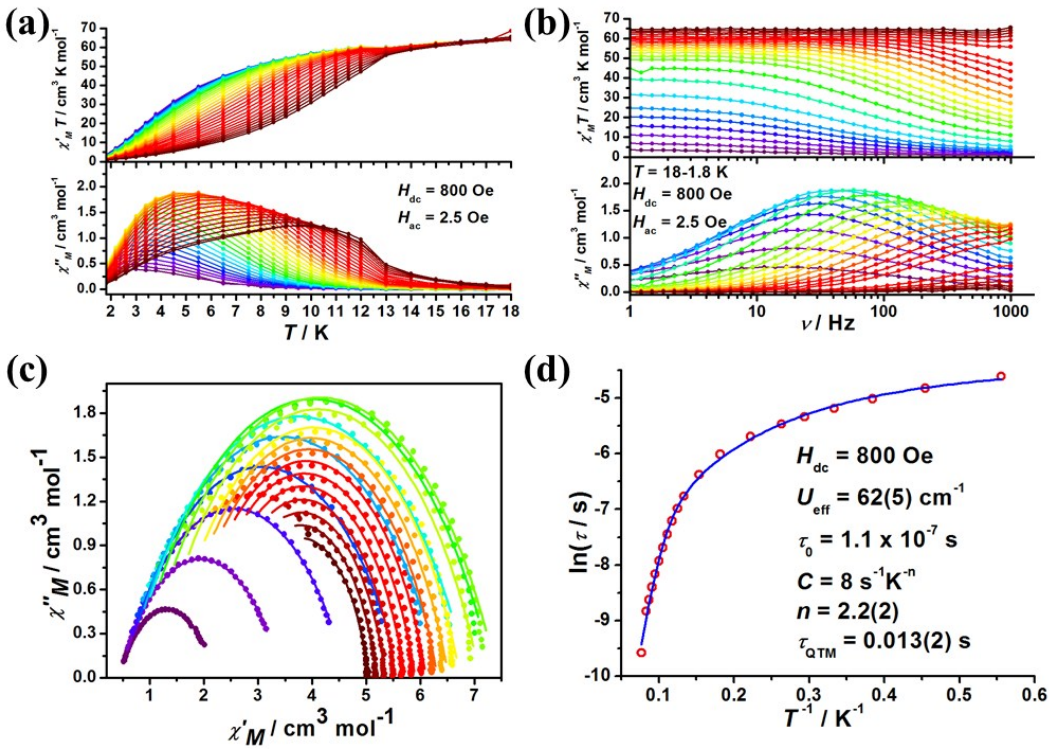

Fig. S11. Alternating current molar magnetic susceptibilities, Cole−Cole plot, and magnetic relaxation for **2**. (a, b) Temperature and frequency dependence of the in-phase ($\chi_M'T$) product and out-of-phase (χ_M'') in 800 Oe dc field for **2** with the ac frequency of 1−1000 Hz. (c) Cole−Cole plot. The solid lines are the best fit to Debye's law. (d) Temperature dependence of the magnetic relaxation time τ under 800 Oe. The solid lines are the best fits to the relaxation equation.

Table S7 Relaxation fitting parameters from Least-Squares Fitting of χ(ω) data for **2** in 800 Oe dc field.

T / K	τ	τ	α	α	χ_0	χ_0	χ_∞	χ_∞
	Value	Standard Error	Value	Standard Error	Value	Standard Error	Value	Standard Error
1.8	0.009989523	7.73E-05	0.386799744	0.002575318	2.199941518	0.004595275	0.43089344	0.003006062

2.2	0.008040818	3.56E-05	0.36833961	0.001574534	3.4299287	0.004305677	0.447866242	0.003232849
2.6	0.006633042	3.03E-05	0.356654721	0.0016883	4.627726241	0.005964115	0.472807694	0.00504503
3	0.005586331	4.06E-05	0.347963428	0.002747748	5.614905507	0.011183732	0.512488777	0.01050371
3.4	0.004804557	4.29E-05	0.344842469	0.003401114	6.351982515	0.014969106	0.554547342	0.015396846
3.8	0.004210298	4.45E-05	0.343586444	0.004025787	6.877904979	0.018398136	0.604353237	0.020489368
4.5	0.003370566	4.29E-05	0.339803252	0.004824336	7.349172815	0.021740618	0.705259587	0.027682689
5.5	0.002445695	3.87E-05	0.328336361	0.00595521	7.417224035	0.023680634	0.876934324	0.03657795
6.5	0.001701729	4.25E-05	0.303398949	0.009438938	7.09756411	0.030082543	1.101575705	0.057723847
7.5	0.001150074	2.41E-05	0.285613748	0.007669546	6.733067737	0.019249676	1.316241792	0.04719207
8	9.27E-04	2.09E-05	0.273954449	0.008082042	6.521816096	0.01760308	1.436794323	0.049624551
8.5	7.40E-04	1.76E-05	0.262801541	0.008274191	6.313180348	0.01549405	1.558108937	0.050930651
9	5.83E-04	1.47E-05	0.251672793	0.008436842	6.102884901	0.013400442	1.680325337	0.052314828
9.5	4.58E-04	1.27E-05	0.239268666	0.008816132	5.901921127	0.011719772	1.817522439	0.05501692
10	3.60E-04	1.08E-05	0.227874467	0.008990095	5.713133095	0.009890188	1.958887646	0.056748912
10.5	2.85E-04	9.19E-06	0.214981109	0.00901451	5.532652735	0.008091393	2.109935574	0.05739275
11	2.26E-04	8.34E-06	0.199771436	0.009602604	5.354217184	0.006914701	2.259637814	0.061593776
11.5	1.79E-04	7.25E-06	0.187800967	0.009586581	5.192070266	0.005495557	2.391686615	0.062867244
12	1.46E-04	7.19E-06	0.170321815	0.010806284	5.035333028	0.004850764	2.542497161	0.070892457
13	6.89E-05	9.18E-06	0.172938283	0.01595426	4.605908867	0.002704718	2.917751401	0.13656072

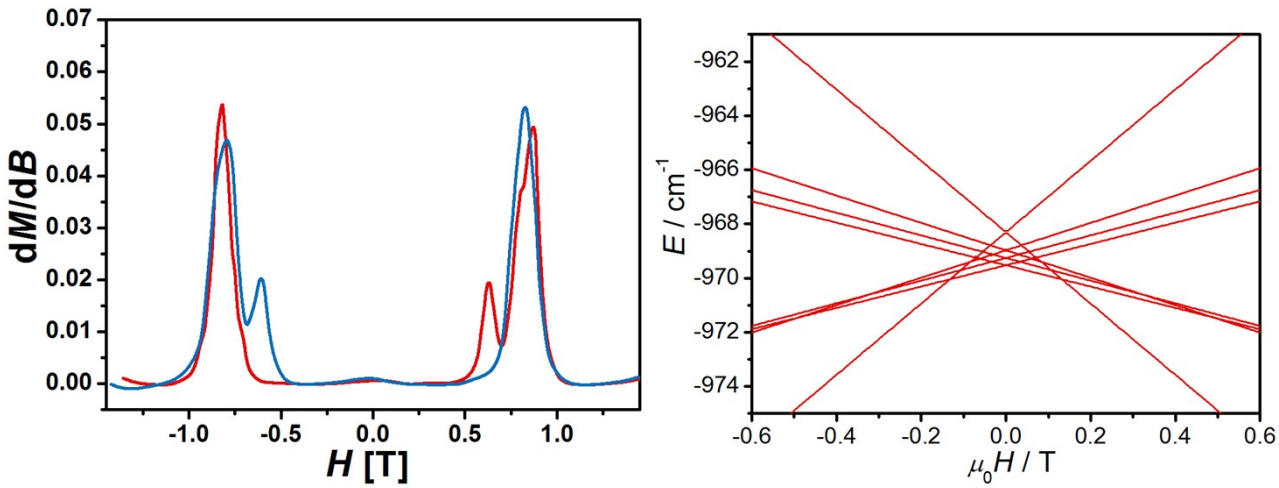

Fig. S12. (left) Derivatives of the hysteresis loops. (right) Zeeman energy diagram for **1**.

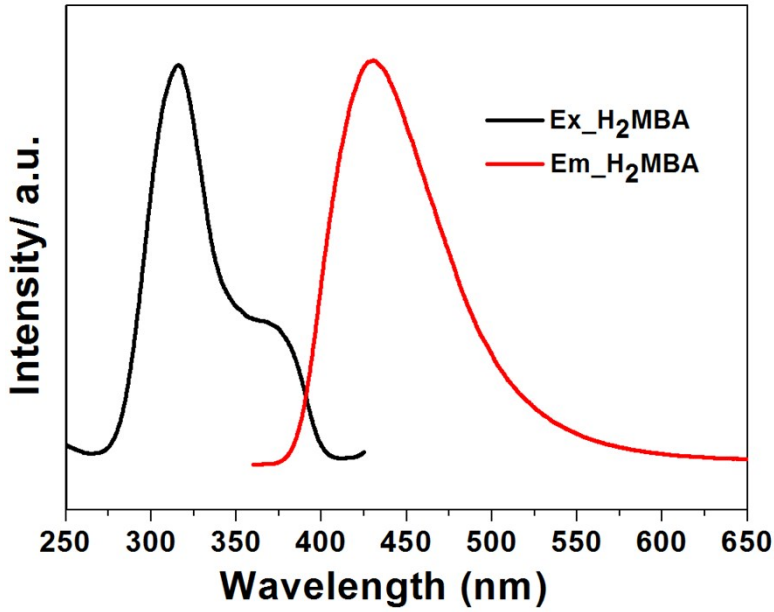

Fig. S13. Solid-state emission spectra of H_2MBA with excitation wavelengths at 320 nm at room temperature.

Computational details

The coordination environments around three Dy(III) ions for **1** are different, and thus we need to calculate three types of Dy(III) fragments indicated as **Dy1−Dy3**. For the three-dimensional chain of complex **2**, we extracted a six-core unit including six types of individual Dy(III) fragments indicated as **Dy1−Dy6**. All of individual Dy(III) fragments (see Figure S7 for the calculated model structures of Dy1 fragments in complexes **1** and **2**) on the basis of single-crystal X-ray determined geometry have been carried out by complete-active-space self-consistent field (CASSCF) with MOLCAS 8.4[4] program package. Each individual Dy(III) fragment in **1** and **4** was calculated keeping the experimentally determined structure of the corresponding compound while replacing the other Dy(III) ions with diamagnetic Lu(III).

The basis sets for all atoms are atomic natural orbitals from the MOLCAS ANO-RCC library: ANO-RCC-VTZP for Dy(III); VTZ for close O; VDZ for distant atoms. The calculations employed the second order Douglas-Kroll-Hess Hamiltonian, where scalar relativistic contractions were taken into account in the basis set and the spin-orbit couplings were handled separately in the restricted active space state interaction (RASSI-SO) procedure. For individual Dy(III) fragment, active electrons in 7 active spaces include all f electrons (CAS(9 in 7 for Dy(III))) in the CASSCF calculation. To exclude all the doubts, we calculated all the roots in the active space. We have mixed the maximum number of spin-free state which was possible with our hardware (all from 21 sextets, 128 from 224 quadruplets, 130 from 490 doublets for Dy(III)). SINGLE_ANISO[5] program was used to obtain the energy levels, g tensors, predominant m_J values, magnetic axes, et al., based on the above CASSCF/RASSI-SO calculations.

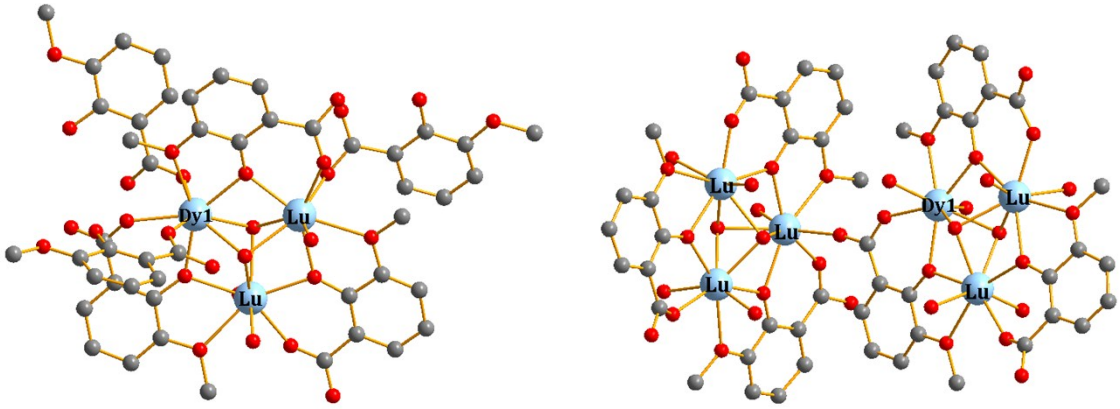

1 **2**

Fig. S14. Calculated model structures of **Dy1** fragments in complexes **1** and **2**; H atoms are omitted.

Table S8. Calculated energy levels (cm^{-1}), ***g*** (g_x, g_y, g_z) tensors and predominant m_J values of the lowest eight Kramers doublets (KDs) of individual Dy^{III} fragments for **1** and **2** using CASSCF/RASSI-SO with MOLCAS 8.4.

KDs	**1_Dy1**			**1_Dy2**			**1_Dy3**		
	E/cm^{-1}	***g***	m_J	E/cm^{-1}	***g***	m_J	E/cm^{-1}	***g***	m_J
1	0.0	0.225 0.679 17.273	±15/2	0.0	0.004 0.007 19.601	±15/2	0.0	0.0462 0.1206 19.1365	±15/2
2	37.3	0.027 0.686 14.509	±11/2	170.9	0.057 0.073 16.630	±13/2	65.6	0.301 0.303 15.975	±13/2
3	138.5	1.724 2.347 13.306	±13/2	321.7	0.365 0.394 13.605	±11/2	144.3	0.819 1.210 13.864	±11/2
4	228.6	3.538 5.632 8.379	±9/2	445.1	1.457 1.999 10.347	±9/2	236.7	2.981 4.452 10.401	±9/2
5	300.6	1.441	±7/2	533.4	6.576	±7/2	331.4	2.731	±7/2

		4.670 9.230			4.925 2.547			5.905 9.896	
6	350.9	1.730 2.694 12.612	±3/2	585.1	2.305 5.102 13.314	±1/2	434.2	0.669 3.368 11.888	±3/2
7	416.9	0.375 0.584 16.325	±5/2	669.3	0.089 0.218 18.014	±3/2	492.1	1.588 2.560 15.040	±5/2
8	528.4	0.047 0.067 19.623	±1/2	772.2	0.005 0.011 19.542	±5/2	534.7	0.396 1.154 18.831	±1/2
KDs	**2_Dy1**			**2_Dy2**			**2_ Dy3**		
	E/cm^{-1}	***g***	m_J	E/cm^{-1}	***g***	m_J	E/cm^{-1}	***g***	m_J
1	0.0	0.002 0.003 19.780	±15/2	0.0	0.078 0.162 19.149	±15/2	0.0	0.008 0.013 19.605	±15/2
2	194.0	0.021 0.029 16.802	±13/2	76.5	0.599 0.883 15.515	±13/2	98.1	0.132 0.165 16.492	±13/2
3	342.3	0.405 0.459 13.816	±11/2	139.1	0.259 1.397 13.068	±11/2	211.9	0.561 0.706 13.738	±11/2
4	458.1	1.081 1.597 10.781	±9/2	235.3	2.986 3.902 10.594	±9/2	324.0	1.200 2.187 10.962	±9/2
5	534.8	1.314 4.092 7.734	±5/2	321.2	8.851 5.412 1.513	±3/2	428.7	2.799 5.068 8.506	±5/2
6	575.6	2.557 6.311 12.909	±1/2	388.3	2.156 3.283 15.076	±5/2	512.4	8.173 5.154 1.235	±7/2
7	655.4	0.117 0.237 18.334	±3/2	468.6	0.316 0.693 17.431	±1/2	547.5	1.847 6.534 12.628	±3/2
8	761.8	0.006 0.015 19.536	±7/2	549.9	0.063 0.125 19.355	±7/2	623.7	0.062 0.321 19.290	±1/2
KDs	**2_ Dy4**			**2_ Dy5**			**2_ Dy6**		
	E/cm^{-1}	***g***	m_J	E/cm^{-1}	***g***	m_J	E/cm^{-1}	***g***	m_J
1	0.0	0.012 0.015 19.737	±15/2	0.0	0.020 0.040 19.383	±15/2	0.0	0.002 0.004 19.544	±15/2
2	117.9	0.457	±13/2	90.3	0.238	±13/2	176.9	0.035	±13/2

		0.697 16.428			0.318 16.258			0.045 16.417	
3	197.7	3.023 3.65 13.4304	±9/2	187.4	0.753 1.082 13.325	±11/2	320.0	0.584 0.729 13.225	±11/2
4	268.0	8.662 6.072 0.261	±11/2	290.7	1.594 2.963 10.707	±9/2	432.9	1.185 1.967 9.884	±9/2
5	358.5	1.497 5.301 9.906	±5/2	377.4	2.695 5.148 8.896	±5/2	504.2	4.813 5.197 8.439	±5/2
6	419.6	2.613 4.603 10.395	±7/2	442.2	1.721 3.853 14.505	±7/2	555.7	1.126 2.554 14.583	±1/2
7	444.2	1.676 6.180 12.142	±3/2	485.0	0.546 1.340 16.593	±1/2	659.2	0.017 0.034 17.966	±3/2
8	530.3	0.089 0.225 19.468	±1/2	553.5	0.087 0.244 19.206	±3/2	760.7	0.003 0.006 19.431	±7/2

Table S9. Wave functions with definite projection of the total moment | m_J > for the lowest two or three KDs of individual Dy^{III} fragments for **1** and **2** using CASSCF/RASSI-SO with MOLCAS 8.4.

	E/cm^{-1}	wave functions
1_Dy1	0.0	57%|±15/2>+25%|±11/2>
	37.3	32%|±13/2>+25%|±11/2>+23%|±9/2>+12%|±7/2>
1_Dy2	0.0	96%|±15/2>
	170.9	88%|±13/2>
	321.7	72%|±11/2>+18%|±7/2>
1_Dy3	0.0	88%|±15/2>
	65.6	78%|±13/2>+11%|±9/2>
2_Dy1	0.0	96%|±15/2>
	194.0	85%|±13/2>+11%|±9/2>
	342.3	59%|±11/2>+22%|±7/2>
2_Dy2	0.0	89%|±15/2>
	76.5	59%|±13/2>+13%|±9/2>+11%|±7/2>
2_Dy3	0.0	95%|±15/2>
	98.1	85%|±13/2>

3_Dy4	0.0	97%|±15/2>
	117.9	86%|±13/2>
3_Dy5	0.0	93%|±15/2>
	90.3	67%|±13/2>
3_Dy6	0.0	95%|±15/2>
	176.9	80%|±13/2>+15%|±9/2>

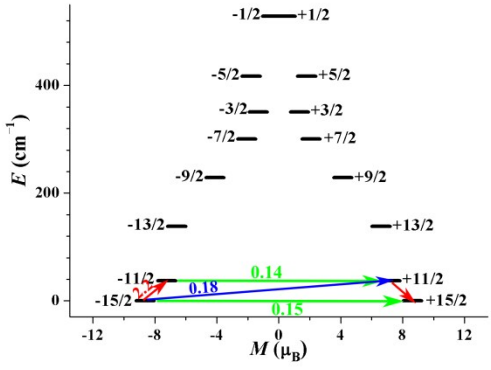

1_Dy1

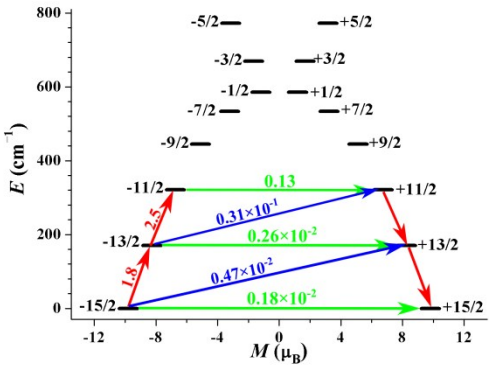

1_Dy2

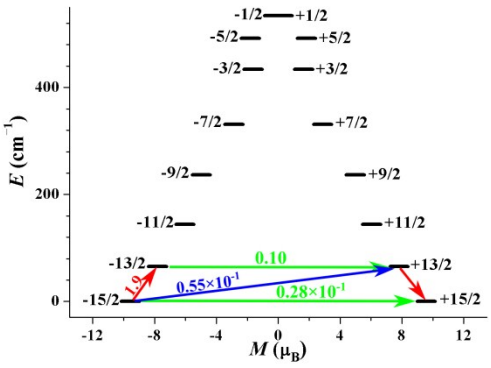

1_Dy3

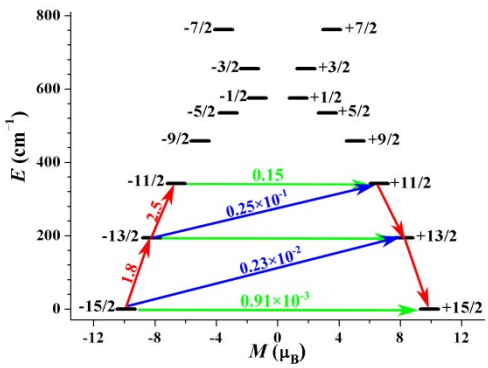

2_Dy1

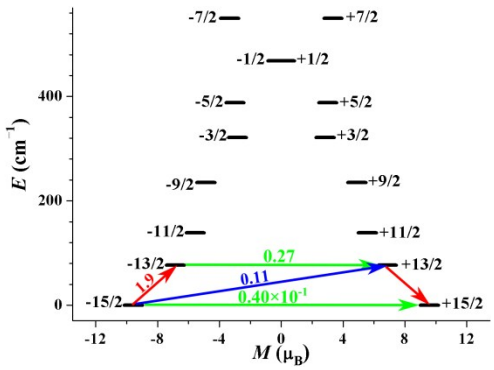

2_Dy2

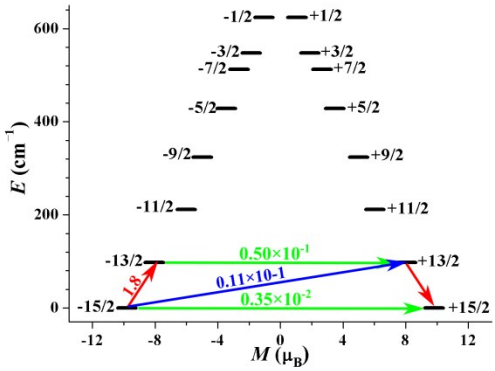

2_Dy3

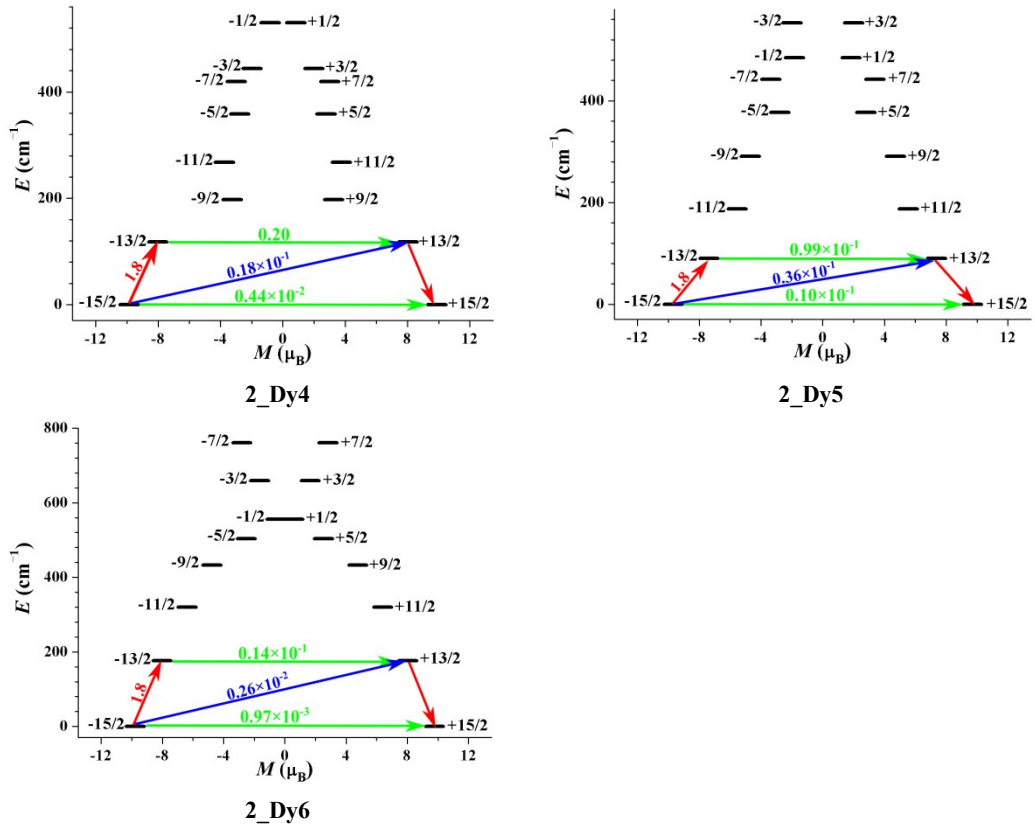

Fig. S15. Magnetization blocking barriers for individual Dy^{III} fragments in complexes **1** and **2**. The thick black lines represent the KDs of the individual Dy^{III} fragments as a function of their magnetic moment along the magnetic axis. The green lines correspond to diagonal matrix element of the transversal magnetic moment; the blue line represent Orbach relaxation processes. The path shown by the red arrows represents the most probable path for magnetic relaxation in the corresponding compounds. The numbers at each arrow stand for the mean absolute value of the corresponding matrix element of transition magnetic moment.

Dy(Ⅲ)-Dy(Ⅲ) exchange interactions

To fit the exchange interactions between Dy(III) ions in complexes **1** and **2**, we took two steps to obtain them. Firstly, we calculated individual Dy(III) fragments using CASSCF/RASSI-SO to obtain the corresponding magnetic properties. Then, the exchange interactions between the magnetic centers are considered within the Lines model,[6] while the account of the dipole-dipole magnetic couplings are treated exactly. The Lines model is effective and has been successfully used widely in the research field of d and f-elements single-molecule magnets.[7]

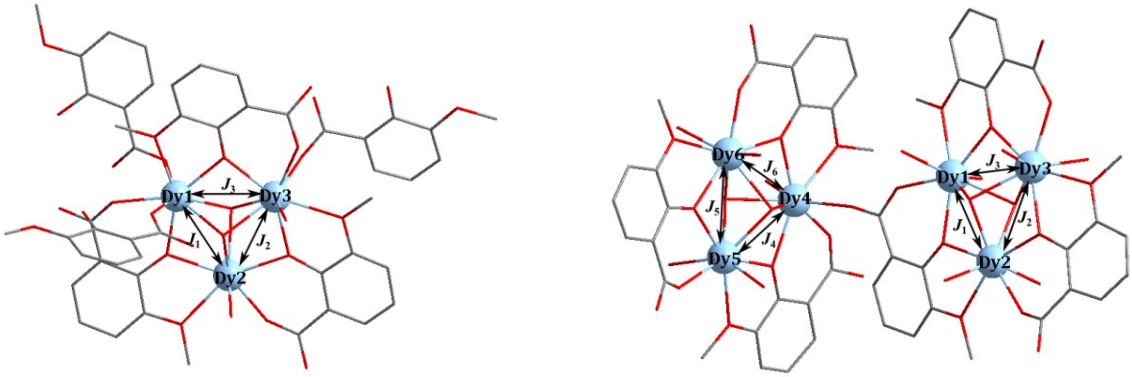

1 **2**

Fig. S16. Scheme of the Dy(III)-Dy(III) interactions in complexes **1** and **2**.

The Ising exchange Hamiltonians are:

$$\hat{H}_{exch} = -J_1 \hat{S}_{Dy1} \hat{S}_{Dy2} - J_2 \hat{S}_{Dy2} \hat{S}_{Dy3} - J_3 \hat{S}_{Dy1} \hat{S}_{Dy3} \quad (1)$$

$$\hat{H}_{exch} = -J_1 \hat{S}_{Dy1} \hat{S}_{Dy2} - J_2 \hat{S}_{Dy2} \hat{S}_{Dy3} - J_3 \hat{S}_{Dy1} \hat{S}_{Dy3} - J_4 \hat{S}_{Dy4} \hat{S}_{Dy5} - J_5 \hat{S}_{Dy5} \hat{S}_{Dy6} - J_6 \hat{S}_{Dy4} \hat{S}_{Dy6} \quad (2)$$

The total J_{total} is the parameter of the total magnetic interaction ($J_{total} = J_{diploar} + J_{exchange}$) between magnetic center ions. The $\tilde{S}_{Dy}$ = 1/2 is the ground pseudospin on the Dy^{III} site. The dipolar magnetic couplings can be calculated exactly, while the exchange coupling constants were fitted through comparison of the computed and measured magnetic susceptibilities using the POLY_ANISO program.[S3]

Table S10. Fitted exchange coupling constants J_{exch}, the calculated dipole-dipole interactions J_{dip} and the J_{total} between magnetic center ions in **1** and **2** (cm^{-1}). The intermolecular interactions zJ' of **1** and **2** were fitted to −0.05 and −0.06 cm^{-1}, respectively.

	1			**2**		
	J_{exch}	J_{dip}	J_{total}	J_{exch}	J_{dip}	J_{total}
J_1	−0.84	−0.25	−1.09	−0.39	−1.92	−2.31
J_2	−0.61	−0.97	−1.58	−0.78	−0.30	−1.08
J_3	−0.67	0.19	−0.48	−0.98	−1.33	−2.31
J_4				−0.86	−1.87	−2.73
J_5				−1.02	−2.08	−3.10
J_6				−0.72	−2.58	−3.30

Table S11. Exchange energies E (cm^{-1}), the energy difference between each exchange doublets Δ_t (cm^{-1}) and the main values of the g_z for the lowest four exchange doublets of **1**−**2**.

	1			**2**		
	E	Δ_t	g_z	E	Δ_t	g_z
1	0.0	0.73×10^{-5}	13.652	0.0	0.19×10^{-7}	7.031
2	0.7	0.66×10^{-4}	36.382	1.6	0.13×10^{-3}	42.899
3	1.0	0.72×10^{-3}	35.164	1.6	0.23×10^{-3}	34.929
4	1.3	0.37×10^{-3}	37.217	2.3	0.47×10^{-6}	38.159

References

1. O. V. Dolomanov, L. J. Bourhis, R. J. Gildea, J. A. Howard and H. Puschmann, *J. Appl. Crystallogr.*, 2009, **42**, 339-341.

2. G. M. Sheldrick, *Acta Crystallographica Section C: Structural Chemistry*, 2015, **71**, 3-8.

3. A. L. Spek, *J. Appl. Crystallogr.*, 2003, **36**, 7–13.

4. (a) G. Karlström, R. Lindh, P.-Å. Malmqvist, B. O. Roos, U. Ryde, V. Veryazov, P.-O. Widmark, M. Cossi, B. Schimmelpfennig, P. Neogrady and L. Seijo, *Comput. Mater. Sci.*, 2003, **28**, 222-239. (b) A. Francesco, A. Jochen,

C. R. K., C. L. F., D. M. G., D. V. Luca, F. G. Ignacio, F. Nicolas, F. L. Manuel, G. Laura, G. Marco, G. Angelo, H. C. E., L. M. Giovanni, L. Hans, M. Dongxia, M. P. Åke, M. Thomas, N. Artur, O. Massimo, P. T. Bondo, P. Daoling, P. Felix, P. Ben, R. Markus, R. Ivan, S. Igor, S.-M. Javier, S. Michael, T. D. G., U. Liviu, V. Alessio, V. Steven, V. Valera, V. V. P., W. Oliver, Z. Felipe and L. Roland, *J. Comput. Chem.*, 2016, **37**, 506-541.

5. (a) L. F. Chibotaru, L. Ungur and A. Soncini, *Angew. Chem. Int. Ed.*, 2008, **47**, 4126-4129. (b) L. F. Chibotaru, L. Ungur, C. Aronica, H. Elmoll, G. Pilet and D. Luneau, *J. Am. Chem. Soc.*, 2008, **130**, 12445-12455.

6. M. E. Lines, *J. Chem. Phys.*, 1971, **55**, 2977-2984.

7. (a) K. C. Mondal, A. Sundt, Y. Lan, G. E. Kostakis, O. Waldmann, L. Ungur, L. F. Chibotaru, C. E. Anson and A. K. Powell, *Angew. Chem. Int. Ed.*, 2012, **51**, 7550-7554. (b) S. K. Langley, D. P. Wielechowski, V. Vieru, N. F. Chilton, B. Moubaraki, B. F. Abrahams, L. F. Chibotaru and K. S. Murray, *Angew. Chem. Int. Ed.*, 2013, **52**, 12014-12019.